Mathematical Biosciences and Engineering

MBE, 23 (6): 1844–1868.
DOI: 10.3934/mbe.2026067
Received: 17 February 2026
Revised: 06 April 2026
Accepted: 20 April 2026
Published: 27 May 2026

http://www.aimspress.com/journal/MBE

Research article

Reinterpreting stochastic optimal control under ecological uncertainty: Inferring decision urgency from vegetation biomass dynamics

Komi Mensah Agboka [1,2,*], Tobias Landmann [1] and Elfatih M. Abdel-Rahman [1,3]

[1] International Centre of Insect Physiology and Ecology (*icipe*), P.O. Box 30772 00100, Nairobi, Kenya.
[2] Laboratoire de Recherche en Science et Technologie (LARSI), Département de Génie Informatique (GI), École Polytechnique de Lomé (EPL), Université de Lomé, Lomé, Togo.
[3] School of Agriculture and Science, University of KwaZulu-Natal, Pietermaritzburg 3209, South Africa.

* **Correspondence:** Email: kagboka@icipe.org/dilaneagboka@gmail.com.

Abstract: Stochastic optimal control provides a rigorous framework for systems subject to uncertainty, yet its operational use in ecological crisis contexts remains limited by interpretability. We reinterpreted a stochastic control formulation in which selected parameters emerged as indicators of decision urgency rather than normative preferences. Vegetation biomass was modeled as a stochastic stock subject to nonlinear loss driven by feeding pressure (e.g., desert locust activity) and multiplicative noise, with uncertainty represented by a time-varying volatility term that integrated extreme rainfall anomalies and conflict-related disruption. Rather than prescribing an optimal policy, we inverted the closed-form solution of the control problem to infer the minimum urgency required to maintain the stock above a policy-defined threshold. Applied spatio-temporally, the framework revealed coherent monthly and regional patterns of inferred urgency, distinguishing stable regimes from disruption-dominated conditions and identifying periods in which short-term depletion overwhelms recovery.

Keywords: optimal control theory; Brownian motion; Hamilton–Jacobi–Bellman; operational decision support; *Schistocerca gregaria*

1. Introduction

Ecological systems exposed to extreme biological shocks often exhibit nonlinear, stochastic, and

path-dependent dynamics that challenge conventional modeling and decision-making frameworks [1]. These impacts arise from complex interactions among biological processes, environmental variability, and human response capacity, leading to abrupt and spatially heterogeneous losses in vegetation biomass that are difficult to anticipate or manage using deterministic or equilibrium-based approaches [2–4]. Outbreaks of highly mobile herbivorous insects, such as desert locusts (*Schistocerca gregaria*), represent a particularly acute manifestation of this challenge [5].

Stochastic process models provide a natural mathematical framework for representing ecological systems that evolve under uncertainty, abrupt fluctuations, and incomplete observability [6–8]. In this context, stochastic differential equations (SDEs) driven by Brownian motion are widely used as reduced-form representations of cumulative, unresolved variability arising from environmental forcing, behavioral heterogeneity, and measurement or surveillance gaps [9–13]. Rather than modeling each source of randomness explicitly, the Brownian component captures their aggregate effect on system dynamics in a tractable way [12].

When combined with optimal control theory, such SDE-based formulations lead to stochastic control problems whose solutions are characterized by Hamilton–Jacobi–Bellman (HJB) equations [9,10]. This framework has been applied to modeled agricultural exploitation and sales planning problems using SDEs to represent production dynamics subject to environmental and market variability, while optimal decisions are derived by solving the associated Hamilton–Jacobi–Bellman equations [14]. However, while mathematically well established, the use of Hamilton–Jacobi–Bellman equations in operational ecological decision support in time and space remains limited, largely because the resulting parameters and policies are often difficult to interpret in biologically or management-relevant terms.

A central reason is not mathematical intractability, but rather interpretability: Key model parameters, such as volatility, elasticity, or discounting, are often difficult to relate directly to biologically meaningful processes or actionable management decisions. This interpretability gap is particularly pronounced under crisis conditions. During extreme biological shocks, decision-makers are rarely interested in long-term optimal trajectories or equilibrium states [15]. Instead, they face urgent questions such as how fast intervention must occur, where losses may become unacceptable, and which locations require immediate prioritization [16]. Traditional stochastic control formulations, while mathematically elegant, typically embed these questions implicitly within abstract optimization objectives, making it difficult to extract decision-relevant insights without strong assumptions about preferences or economic valuation.

In this study, we argued that this limitation stems not from the stochastic control framework, but from how its parameters are commonly interpreted. Rather than treating quantities such as discount rates or loss elasticities as fixed economic or biological constants, we propose a reinterpretation in which these parameters are viewed as emergent indicators of decision urgency under uncertainty. In classical stochastic optimal control, the discount rate r is introduced as a temporal weighting parameter that determines how future outcomes are valued relative to present ones, thereby directly influencing optimal decisions and stopping behavior under uncertainty [17]. Beyond this economic interpretation, r plays a structural role in dynamic programming formulations, where it governs the time sensitivity of the value function and the responsiveness of optimal trajectories through the Hamilton–Jacobi–Bellman equation [18]. Consequently, changes in the discount rate systematically alter the balance between short-term and long-term dynamics, effectively controlling how rapidly decisions respond to evolving system states.

Within this perspective, stochastic control models are not viewed as normative prescriptions of

an optimal exploitation problem, but a potential diagnostic tool to translate ecological variability and operational constraints into interpretable measures of response pressure. Therefore, we developed and illustrated this reinterpretation using vegetation biomass dynamics in Sudan as a representative ecological system exposed to interacting environmental shocks and management constraints. Herbivory pressure, exemplified here by desert locust feeding, exhibits pronounced nonlinearity with consumption rates that saturate at high resource availability due to physiological and behavioral constraints [19–21], while rainfall extremes, temperature suitability, and disruptions to monitoring and control operations further modulate biomass depletion [22–25]. To address these coupled dynamics, we represent vegetation biomass as a stochastic stock process [14] subject to nonlinear, saturation-limited losses [26], and multiplicative environmental noise, and invert the resulting stochastic control solution to infer the minimum level of decision urgency required to prevent biomass stocks from falling below a policy-defined acceptable threshold.

2. Materials and methods

To operationalize the stochastic control framework with biologically interpretable inputs, we construct (i) a biological saturation factor $\gamma(t)$ from normalized difference vegetation index (NDVI)-derived biomass using a Holling-type saturation form with parameter uncertainty propagated by Monte Carlo sampling, and (ii) a time-varying volatility $\sigma(t)$ derived from an instability index combining operational disruption, rainfall extremes, and background habitat suitability (Figure 1). These quantities are then coupled to the closed-form optimal stock trajectory and inverted numerically to infer the implied urgency parameter $\sigma(t)$ required to keep the stock above a specified target level M_t^{tar} under stochastic forcing.

2.1. Stochastic representation of resource stock dynamics and inversion of the optimal stock trajectory to infer policy urgency

We model vegetation biomass in Sudan as a continuous-time stochastic stock process subject to herbivory-driven depletion and environmental uncertainty, with desert locust feeding used as a representative loss mechanism. Sudan is used as a motivating case study because it represents a highly variable, shock-prone system where vegetation dynamics, desert locust pressure, and severe insecurity interact strongly across space and time. Sudan lies within a region that has been repeatedly affected by desert locust invasion [27–30]. Vegetation productivity is largely rainfall-driven, making biomass availability sensitive to short-term climatic anomalies that can rapidly amplify locust breeding potential [31]. Furthermore, conflicts have introduced pronounced spatial heterogeneity in surveillance and response capacity across states, creating conditions where biological pressure and operational constraints may align [32]. This combination makes Sudan a suitable test case for demonstrating a stochastic decision framework that links biological buffering, environmental instability, and intervention urgency, without aiming to predict realized impacts or losses.

Let us denote the total vegetation biomass stock available at time t. The stochastic differential equation describes its temporal evolution as follows [9–11]:

$$dM_t = -v(t, M_t)dt + \sigma M_t dW_t, M(0) = M_0, \tag{1}$$

where $v(t, M_t)$ is the control variable representing the rate of vegetation biomass loss

attributable to locust consumption, σ is a volatility parameter capturing uncertainty in loss intensity, and W_t is a standard Wiener process. The stochastic term captures the erratic, unpredictable nature of desert locust swarm behavior and damage intensity.

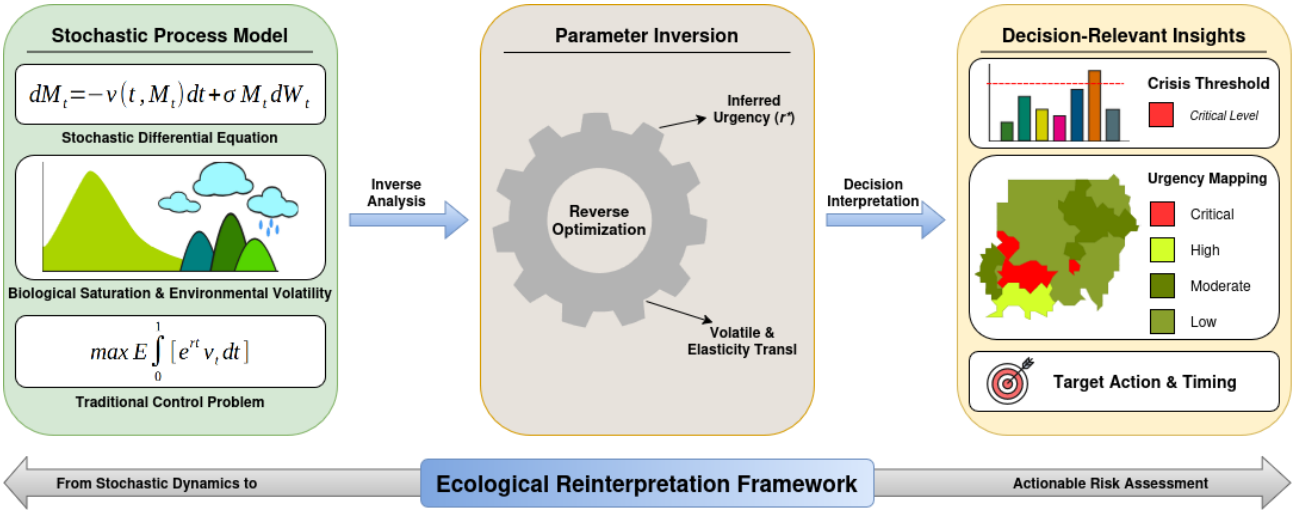

Figure 1. The components and their implications for decision-relevant stock vulnerability. Panel (a) reports $\gamma(t)$ with uncertainty bands arising from uncertainty in the Holling/allometric parameters, rather than variability from individual Brownian sample paths. Panel (b) shows the constructed $\sigma(t)$ trajectory under the chosen shock regime, while panel (c) presents the corresponding inferred $r(t)$ obtained by numerically inverting the policy kernel at each time point given $\gamma(t)$, $\sigma(t)$, and the target constraint.

2.1.1. Optimal control formulation

We characterize biomass stock vulnerability under crisis conditions by formulating a stochastic control problem that represents extreme consumption pressure rather than a normative management objective. Specifically, we consider a discounted utility functional of locust-driven biomass loss, defined as:

$$\max_{v} \mathbb{E}\left[\int_0^T e^{-rt} v_t^{\gamma} dt\right], \tag{2}$$

subject to the stock dynamics above, where $r > 0$ is a discount rate and $0 < \gamma < 1$ represents the elasticity of loss intensity. This formulation does not imply the desirability of biomass loss but provides a mathematically tractable abstraction of worst-case exploitation pressure arising from interacting biotic and abiotic stressors, such as locust feeding, climatic extremes, and operational disruption, thereby enabling inversion of the control solution to infer the minimum decision urgency required to maintain biomass above a policy-defined threshold under uncertainty.

2.1.2. Optimal policy and stock trajectory

Following standard results in stochastic optimal control theory, the above problem admits a closed-form optimal control policy. As the derivation follows established arguments, it is not reproduced here (see Diallo et al. [14], for details). The resulting optimal control is given by:

$$v^*(t, M_t) = \left(\frac{\alpha}{1-\gamma}\right) \frac{M_t}{1 - \exp\left[-\left(\frac{\alpha}{1-\gamma}\right)(T-t)\right]}, \tag{3}$$

with:

$$\alpha = r - \frac{1}{2}\sigma^2\gamma(\gamma - 1). \tag{4}$$

Substituting this control into the state equation yields the corresponding optimal biomass stock trajectory

$$M_t^* = M_0 \left[\frac{1 - \exp\left(-\frac{\alpha}{1-\gamma}(T-t)\right)}{\exp\left(\frac{\alpha}{1-\gamma}t\right) - \exp\left(-\frac{\alpha}{1-\gamma}(T-t)\right)}\right] \exp\left(-\frac{1}{2}\sigma^2 t + \sigma W_t\right). \tag{5}$$

These expressions describe the expected depletion dynamics of vegetation biomass under sustained desert locust feeding pressure and stochastic environmental variability. The biomass stock process is evaluated up to the first time at which M_t reaches zero, corresponding to complete depletion of available vegetation. This event defines a crisis threshold beyond which ecosystem functioning collapses and is used to interpret early stock exhaustion in the numerical simulations. No recovery dynamics are assumed beyond this point, reflecting worst-case conditions during a locust upsurge.

2.2. Inversion of the optimal stock trajectory to infer policy urgency

We begin from the closed-form optimal stock trajectory obtained from the stochastic control problem:

$$M_t^* = M_0 \left[\frac{1 - \exp\left(-\frac{\alpha}{1-\gamma}(T-t)\right)}{\exp\left(\frac{\alpha}{1-\gamma}t\right) - \exp\left(-\frac{\alpha}{1-\gamma}(T-t)\right)}\right] \exp\left(-\frac{1}{2}\sigma^2 t + \sigma W_t\right), t \in (0, T]. \tag{6}$$

Here, M_0 denotes the initial stock level, σ is the volatility parameter, W_t is a standard Brownian motion, $0 < \gamma < 1$ represents the elasticity of loss intensity, $r > 0$ is the discount rate, and

$$\alpha = r - \frac{1}{2}\sigma^2\gamma(\gamma - 1). \tag{7}$$

Step 1: Definition of a policy urgency parameter

The time-dependent fraction in Eq (6) depends on the parameters only through the ratio $\alpha/(1-\gamma)$. To simplify notation and interpretation, we define the composite parameter

$$k \equiv \frac{\alpha}{1-\gamma} = \frac{r - \frac{1}{2}\sigma^2\gamma(\gamma-1)}{1-\gamma}. \tag{8}$$

Parameter $k > 0$ aggregates the effects of decision urgency (r), uncertainty (σ), and nonlinear loss elasticity (γ).

Substituting Eq (8) into Eq (6) yields

$$M_t^* = M_0 \left[\frac{1 - e^{-k(T-t)}}{e^{kt} - e^{-k(T-t)}}\right] \exp\left(-\frac{1}{2}\sigma^2 t + \sigma W_t\right). \tag{9}$$

Step 2: Deterministic policy kernel

We define the deterministic function

$$G(t;k) = \frac{1 - e^{-k(T-t)}}{e^{kt} - e^{-k(T-t)}}, \tag{10}$$

which captures the policy-driven evolution of the stock.

Eq (9) can then be written compactly as

$$M_t^* = M_0 G(t;k) \exp\left(-\frac{1}{2}\sigma^2 t + \sigma W_t\right). \tag{11}$$

Step 3: Separation of stochastic and policy components

We define the stochastic multiplier

$$Z_t = \exp\left(-\frac{1}{2}\sigma^2 t + \sigma W_t\right) \tag{12}$$

so that the optimal stock trajectory can be expressed as

$$M_t^* = M_0 G(t;k) Z_t \tag{13}$$

This decomposition separates realized stochastic shocks, captured by Z_t, from policy-controlled dynamics, captured by $G(t;k)$.

Step 4: Normalization and target stock constraint

Let M_t^{tar} denote a minimum acceptable stock level at time t. Normalizing Eq (13) yields

$$y \equiv \frac{M_t^{\text{tar}}}{M_0 Z_t} \leq G(t;k), \tag{14}$$

Substituting the definition of $G(t;k)$ gives

$$y = \frac{1 - e^{-k(T-t)}}{e^{kt} - e^{-k(T-t)}}, \tag{15}$$

Step 5: Numerical inversion for the urgency parameter

Eq (15) contains k in exponentials with different arguments and therefore does not admit a closed-form solution in elementary functions. We thus determine k numerically as the unique positive root of the scalar function

$$F(k) = G(t;k) - y, k > 0. \tag{16}$$

The monotonicity of $G(t;k)$ in k guarantees the existence and uniqueness of the solution. In practice, k is obtained using a stable one-dimensional root-finding algorithm (e.g., bisection or Brent's method).

In the numerical implementation, the uncertainty in $\gamma(t)$ is not propagated through the inversion procedure. Instead, the mean trajectory $\gamma_{mean}(t)$ is used to compute the urgency parameter. As a result, the inferred values of $r(t)$ reflect stochastic variability arising from the process-level dynamics (through $\sigma(t)$ and Z_t), but do not incorporate uncertainty associated with the biological saturation parameter. This separation enables a clearer interpretation of the respective contributions of biological and stochastic components.

Step 6: Recovery of the implied discount rate

Once k has been estimated, the implied policy urgency, expressed as a discount rate, follows directly from Eq (8):

$$r = (1-\gamma)k + \frac{1}{2}\sigma^2\gamma(\gamma - 1). \tag{17}$$

This inversion enables r to be interpreted as the degree of urgency required to prevent the stock from falling below a specified target level under stochastic shocks, rather than as an exogenously imposed economic preference.

In standard intertemporal models, r determines the value of future flows and encodes the relative importance of immediate versus delayed outcomes [33,34]. A higher r value reduces the contribution of future states, effectively prioritizing short-term dynamics and accelerating optimal responses to current conditions [33,35,36]. In stochastic control settings, this temporal weighting directly shapes the optimal policy and resulting state trajectory.

The r in this framework should not be interpreted as a biological parameter, nor as a conventional economic preference rate. Instead, it emerges endogenously as an implied policy urgency, defined by the requirement that vegetation biomass stocks remain above a minimum acceptable threshold under stochastic desert locust pressure. From a control-theoretic perspective, this inversion repositions r as a quantity that enforces feasibility of a constrained trajectory. In this sense, r acts is analogous to a dual variable associated with maintaining the system above a prescribed threshold, translating temporal weighting into a measure of constraint pressure. This interpretation is consistent with broader results showing that discounting parameters fundamentally influence optimal stopping and control behavior in stochastic systems [17]. In this sense, r is not estimated from biological

processes such as locust fecundity, development, or mortality, but is inferred from the dynamics of the stock constraint itself. Specifically, r represents the level of decision urgency necessary to prevent the biomass stock M_t from falling below a prescribed target M_t^{tar} at a given time t, given the combined effects of biological saturation, environmental variability, and operational disruption.

Under this interpretation, larger values of r indicate situations in which short-term losses dominate system dynamics, corresponding to emergency-level conditions that require rapid and decisive intervention. Conversely, smaller values of r reflect greater tolerance for delayed impacts and are consistent with longer-term planning and lower perceived urgency. The r thus functions as a quantitative indicator of crisis severity and response pressure, translating stochastic biological shocks into a decision-relevant measure of urgency rather than representing intrinsic economic preferences. This reinterpretation enables the stochastic control framework to operate as a decision-support tool, linking ecological instability directly to actionable assessments of response timing.

2.3. Construction of model parameters and numerical implementation

2.3.1. Vegetation resource proxy

Vegetation availability is represented by a biomass proxy derived from the remotely sensed NDVI. Following established empirical relationships, vegetation biomass at time t is approximated as [37,38]:

$$R(t) = \max(11750 \cdot \mathrm{NDVI}(t) - 3120, \quad 0), \tag{18}$$

where the truncation at zero ensures biological plausibility by preventing negative biomass values. This proxy is used consistently for initial stock estimation and temporal dynamics. The NDVI–biomass relationship adopted here was derived from studies conducted in Senegal. Although geographically distinct, Senegal and the study area share important ecological characteristics as part of the Sudano–Sahelian belt, including strong rainfall seasonality and dryland vegetation dynamics. We therefore considered this relationship as a reasonable approximation for representing biomass variability in the absence of locally calibrated formulations, while acknowledging that regional deviations may exist. Long-term average administrative level NDVI from June to September (2002-2026) is obtained from the Humanitarian Data Exchange (HDX; https://data.humdata.org/dataset/sdn-ndvi-subnational) platform. The datasets were accessed in January 2026 and correspond to the most recent publicly available facility layers for Sudan at the time of data retrieval. The data are available at the second administrative units aggregated to the state (Admin-1).

2.3.2. Biological saturation of consumption pressure

To capture the diminishing marginal impact of feeding pressure as vegetation availability increases, we introduce a biological saturation parameter based on a Holling type II functional form [26]. The saturation factor $\gamma(t)$ is defined as:

$$\gamma(t) = \frac{1}{1 + ahR(t)}, \tag{19}$$

where a denotes an effective attack rate and h represents a handling-time-like parameter. This

formulation reflects physiological limits on intake, spatial aggregation of feeding, and behavioral constraints, ensuring that effective pressure on the resource saturates at high biomass.

2.3.3. Allometric representation and uncertainty propagation

Rather than fixing a and h determining them deterministically, we express them through uncertain allometric relationships,

$$a = a_0 M_{\text{pred}}^{Q_a}, I_{\max} = I_0 M_{\text{pred}}^{Q_I}, h = \frac{1}{I_{\max}}, \tag{20}$$

where M_{pred} is a representative insect body mass (normalized to unity), and a_0 and I_0 are scaling constants. The allometric exponents are treated as uncertain and sampled from normal distributions,

$$Q_a \sim \mathcal{N}(\mu_{Q_a}, \sigma_{Q_a}), Q_I \sim \mathcal{N}(\mu_{Q_I}, \sigma_{Q_I}), \tag{21}$$

with parameter values drawn from published meta-analyses of insect functional responses [39].

Uncertainty in $\gamma(t)$ is propagated using a Monte Carlo simulation. For each NDVI value, an ensemble of $\gamma(t)$ realizations are generated, from which the mean and selected quantiles (2.5%,50%,97.5%) are retained:

$$\gamma_{\text{mean}}(t) = \mathbb{E}[\gamma(t)], \gamma_p(t) = \text{ Quantile }_p(\gamma(t)), \tag{22}$$

These summaries represent uncertainty in biological saturation while avoiding overinterpretation of individual stochastic realizations. Although uncertainty in $\gamma(t)$ is quantified through Monte Carlo simulation and summarized using quantiles, the inversion procedure is performed using the mean trajectory $\gamma_{mean}(t)$. This choice ensures a tractable and interpretable estimation of urgency parameter $r(t)$ while avoiding the compounding of multiple sources of uncertainty within the inversion step.

2.3.4. Time-varying volatility parameter sigma ($\sigma(t)$)

Stochastic variability in stock dynamics is governed by a time-dependent volatility parameter $\sigma(t)$, which captures unresolved sources of variability including erratic swarm behavior, patchy feeding, weather-driven activity bursts, detection gaps, and operational disruptions.

We define an instability index $S(t) \in [0,1]$ as a weighted combination of three interpretable components,

$$S(t) = w_{\text{ops}} S_{\text{ops}}(t) + w_{\text{rain}} S_{\text{rain}}(t) + w_T S_T(t), w_{\text{ops}} + w_{\text{rain}} + w_T = 1, \tag{23}$$

where:

- $S_{\text{ops}}(t)$ is a binary indicator of operational disruption (e.g., conflict or surveillance breakdown) obtained from current knowledge of a war-affected area,

- $S_{\text{rain}}(t)$ flags rainfall extremes, defined as:

$$S_{\text{rain}}(t) = \begin{cases} 1, & \text{if rainfall percentile } \leq 0.10(\text{drought}) \text{ or } \geq 0.95(\text{flood}) \\ 0, & \text{otherwise} \end{cases}, \quad (24)$$

In the baseline specification, equal weights are assigned to all components, i.e., $w_{\text{ops}} = w_{\text{rain}} = w_T = 1/3$. This choice reflects a non-informative and transparent starting point in the absence of strong empirical or theoretical evidence to support differential weighting among drivers. Equal weighting is commonly used in composite indicator construction to avoid introducing subjective bias when relative importance is uncertain [40,41]. We acknowledge that the relative contribution of these components may vary across contexts, and that alternative weighting schemes could influence the magnitude of the resulting volatility index. However, the present formulation is designed to provide a flexible and generalizable framework, in which weights can be readily adjusted based on expert knowledge, empirical calibration, or application-specific priorities. Sensitivity to weighting assumptions is therefore an important consideration for future extensions of the model.

Average rainfall data at administrative level from June to September (2010-2019) were obtained from the Humanitarian Data Exchange (HDX; https://data.humdata.org/) platform. The datasets were accessed in January 2026 and correspond to the most recent publicly available facility layers for Sudan at the time of data retrieval. Rainfall data originally available at finer administrative units were aggregated to the state (Admin-1) level using area-weighted means to ensure consistency with NDVI data, which are reported directly at the state level. Prior to aggregation, administrative name inconsistencies and spelling variants across datasets were manually reconciled using a standardized crosswalk to avoid misclassification.

Desert locust breeding suitability is represented using a bounded species distribution model (SDM) trained with Maximum entropy (MaxEnt), based on temperature, rainfall, and vegetation covariates from Kimathi et al. [27]. The resulting suitability index $S_T(x, m) \in [0,1]$ provides a spatial proxy for desert locust physiological activity. This static suitability raster is overlaid with state boundaries, and area-weighted mean suitability values were extracted per state and treated as a time-invariant covariate across all months.

The volatility parameter was then mapped linearly as:

$$\sigma(t) = \sigma_{\min} + (\sigma_{\max} - \sigma_{\min})S(t) \quad (25)$$

with $\sigma_{\min} = 0.10$ and $\sigma_{\max} = 0.40$. Scenario values (low, medium, high) are defined reproducibly using empirical quantiles of $\sigma(t)$.

For the temporal and spatial analysis, the terminal acceptable stock level M^{tar} is fixed as a 20% of M_t and applied uniformly to all selected locations, providing a common benchmark for evaluating vulnerability under heterogeneous environmental and operational conditions. In addition, the baseline stock M_0 was defined for each state as the mean biomass estimated from NDVI across the seasonal observation window. Because NDVI and biomass vary substantially from month to month due to rainfall, phenology, and land-surface dynamics, using a time-averaged biomass ensures that M_0 represents a characteristic or expected resource level rather than transient conditions. This stable baseline enables policy targets and inferred decision urgency to be interpreted as deviations from normal ecological capacity rather than short-term fluctuations.

Although the stock dynamics are stochastic, results are summarized using conditional

expectations and uncertainty bands rather than individual sample paths. Biological uncertainty $\gamma(t)$ was propagated explicitly through Monte Carlo simulation, while stochastic forcing $\sigma(t)$ was represented via scenario contrasts and inferred policy urgency. This approach avoids path-specific overinterpretation while preserving the influence of uncertainty on decision-relevant quantities. Parameters $\gamma(t)$ and $\sigma(t)$ feed directly into the stochastic control solution, which is inverted numerically to infer the implied discount rate $r(t)$. In this framework, r is not a biological parameter; it represents the urgency of decision-making required to prevent stocks from falling below a specified target.

In the theoretical formulation, the normalization term > $y = \frac{M_t^{\text{tar}}}{M_0 Z_t}$ > depends on the stochastic multiplier $Z_t = \exp\left(-\frac{1}{2}\sigma^2 t + \sigma W_t\right)$, implying that y, and therefore the inferred parameter k, are stochastic quantities. In the numerical implementation, stochasticity is handled through an explicit simulation of the Brownian motion process. Specifically, for each spatial unit, a discrete-time realization of W_t was generated, and the corresponding trajectory of Z_t was computed using the time-varying volatility σ_t. The inversion was then performed pointwise in time using this realized trajectory. That is, for each time step t, the value of y was computed using the simulated Z_t, and parameter k was obtained as the unique root of Eq (16). $r(t)$ is subsequently recovered from k. Consequently, the inferred urgency $r(t)$ represents a path-dependent realization of decision urgency under stochastic forcing, rather than an expectation or a distributional summary. This approach preserves the temporal structure of stochastic variability and enables the model to capture dynamically evolving ecological uncertainty. To ensure reproducibility, all stochastic simulations were performed using a fixed random seed. We note that alternative formulations are possible, including expectation-based or quantile-based inversion schemes, which would yield mean-field or risk-sensitive estimates of urgency. However, this implementation prioritizes trajectory-level interpretation to reflect realized system dynamics under uncertainty.

2.4. Spatio-temporal extension of the framework

To extend the framework from a purely temporal representation to a spatially explicit analysis, we linked the model outputs to Sudan's administrative units using standardized administrative boundary shapefiles (obtained from the Humanitarian Data Exchange (HDX); https://data.humdata.org/dataset/sudan-administrative-boundaries-2 accessed in January 2026). This spatial referencing enables a mean spatio-temporal evaluation at the administrative level, enabling systematic visualization and comparison across regions. Our objective was to assess how biological pressure, environmental instability, and inferred policy urgency vary across space under heterogeneous conditions.

Rather than explicitly simulating spatial stock diffusion, space was treated as a collection of locations indexed by administrative unit, each characterized by locally observed environmental and operational conditions. Temporal dynamics were evaluated at an average of monthly resolution, producing spatially explicit estimates of model quantities. In this way, the spatial extension transforms the stochastic control framework into a scalable decision-support tool that integrates remote sensing, climate variability, and biological constraints into interpretable, decision-relevant indicators of response timing.

As stated above, the inferred discount rate represents the degree of decision urgency required to prevent resource stocks from falling below a specified target level under local stochastic conditions. Rather than interpreting the absolute values of r in isolation, we adopted a relative, data-driven classification that facilitates policy interpretation and comparison across space and time. Specifically, we classified policy urgency using empirical quantiles of the inferred distribution. This approach avoids arbitrary threshold selection, accommodates spatial heterogeneity, and aligns with standard risk stratification practices in climate and disaster risk assessment.

Let $\mathcal{R} = \{r(x,m)\}$ denote the set of inferred urgency values across all spatial locations and months. We defined the following thresholds based on the empirical distribution of $\mathcal{R}$:

$$\begin{aligned} &r_{Q25} = 25 \text{ th percentile of } \mathcal{R}, \\ &r_{Q50} = 50 \text{ th percentile (median) of } \mathcal{R}, \\ &r_{Q75} = 75 \text{ th percentile of } \mathcal{R}. \end{aligned} \tag{26}$$

Using these thresholds, each location and month was assigned to one of four policy urgency categories:

$$\text{Urgency class } (x,m) = \begin{cases} \text{Low}, & r(x,m) \le r_{Q25} \\ \text{Moderate}, & r_{Q25} < r(x,m) \le r_{Q50} \\ \text{High}, & r_{Q50} < r(x,m) \le r_{Q75} \\ \text{Critical}, & r(x,m) > r_{Q75} \end{cases} \tag{27}$$

This classification admits a direct operational interpretation. Areas classified as low urgency are characterized by relatively slow depletion dynamics, enabling longer-term planning, routine monitoring, and preventive measures. Moderate urgency regions require heightened surveillance and preparedness but do not warrant immediate intervention. High urgency regions indicate accelerated depletion risk, where a timely and coordinated response becomes necessary to avoid unacceptable biomass loss. Finally, critical urgency regions correspond to emergency conditions in which short-term losses dominate, and rapid, resource-intensive action is required to prevent irreversible depletion. Importantly, the framework does not prescribe specific interventions; rather, it provides a quantitative lens through which the relative severity of conditions can be assessed across space and time.

The spatial representation adopted in this study is based on administrative units, which provide a consistent and policy-relevant framework for integrating heterogeneous datasets. However, we acknowledge that aggregating spatial data at this level may mask fine-scale variability in vegetation dynamics and locust pressure. This limitation is related to the modifiable areal unit problem (MAUP), whereby statistical results may depend on the scale and configuration of spatial units used in the analysis [42]. The chosen resolution reflects a trade-off between data availability, computational tractability, and decision relevance.

3. Results

Figure 2 illustrates the monthly evolution of biological saturation $\gamma(t)$ across Sudanese states from June to September, derived from NDVI-based biomass estimates. Across most states, $\gamma(t)$ exhibits a pronounced early-season peak, followed by a rapid decline later in the season if M^{tar} is fixed

as a 20% of M_t. States such as Aj Jazirah, Central Darfur, Gedaref, West Darfur, and White Nile showed values of $\gamma(t)$ close to unity in June–July, indicating strong biological saturation consistent with low effective resource limitation. As the season progresses, declining NDVI leads to sharp reductions in $\gamma(t)$, reflecting increasing resource constraint. In contrast, arid and semi-arid regions (Northern, River Nile, Kassala, Red Sea) display persistently flat and near-constant saturation profiles, consistent with chronically low vegetation availability and limited seasonal variability. Intermediate dynamics are observed in Blue Nile, Sennar, South Darfur, and South Kordofan, where $\gamma(t)$ decreases more gradually over time, indicating a slower transition from resource-rich to resource-limited conditions. Importantly, $\gamma(t)$ is a biophysical state variable, not a measure of risk, impact, or hazard occurrence. It represents the degree to which available biomass can buffer depletion processes and enters the model as a modifier of how rapidly policy-relevant stock levels respond to extraction and stochastic shocks. As such, high values of $\gamma(t)$ indicate biological buffering capacity, whereas low values signal heightened sensitivity of the system to perturbations, but do not imply the presence or absence of adverse events.

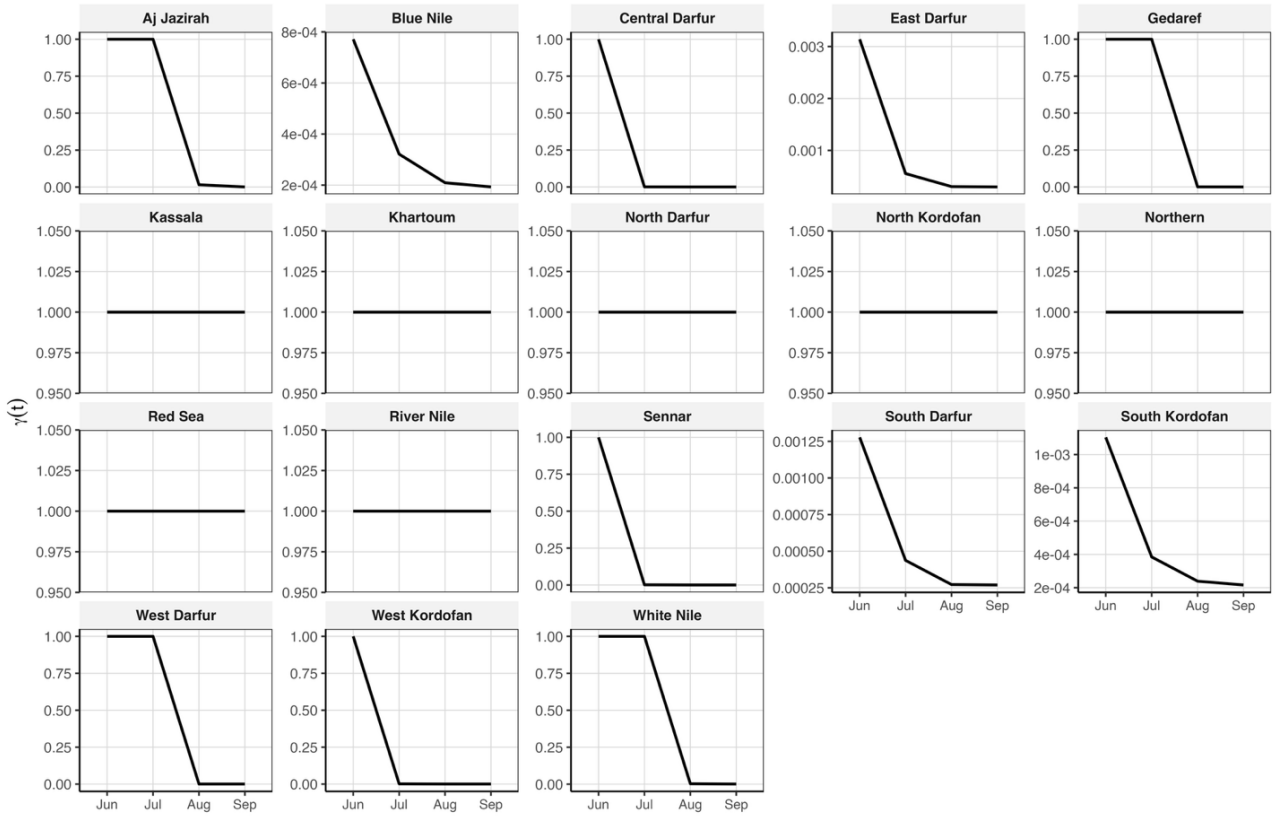

Figure 2. State-level temporal profiles of biological saturation $\gamma(t)$ from June to September. Each panel corresponds to one administrative unit. Biological saturation is derived from normalized difference vegetation index (NDVI)-based biomass estimates and reflects the degree of resource availability relative to depletion pressure. Values near 1 indicate strong biological buffering, while lower values indicate increasing resource limitation.

Figure 3 shows the monthly evolution of the shock volatility term $\sigma(t)$ across Sudanese states from June to September. Volatility reflects the combined influence of conflict exposure, rainfall extremes, and climatic suitability, and captures the intensity of short-term stochastic perturbations acting on the system if M^{tar} is fixed as a 20% of M_t. Across most states, $\sigma(t)$ exhibits marked intra-seasonal variability, with mid-to-late season peaks coinciding with periods of heightened rainfall extremes and persistent operational disruption. Several states (Central Darfur, East Darfur, North Darfur, North Kordofan, Sennar, South Darfur, South Kordofan, and White Nile) display a monotonic increase in volatility toward August–September, indicating growing exposure to compounding shocks as the season progresses. In contrast, arid or conflict-stable regions (Northern, Kassala, River Nile, Red Sea) show comparatively lower and more stable volatility profiles, consistent with weaker rainfall variability and reduced shock amplification. Importantly, $\sigma(t)$ does not represent realized damage, losses, or impact occurrence. Rather, it quantifies the magnitude of uncertainty and shock intensity entering the stochastic stock dynamics. High values of $\sigma(t)$ imply greater unpredictability and stronger short-term fluctuations, which amplify the urgency of decision-making when combined with low biological saturation and binding policy constraints, but do not indicate adverse outcomes.

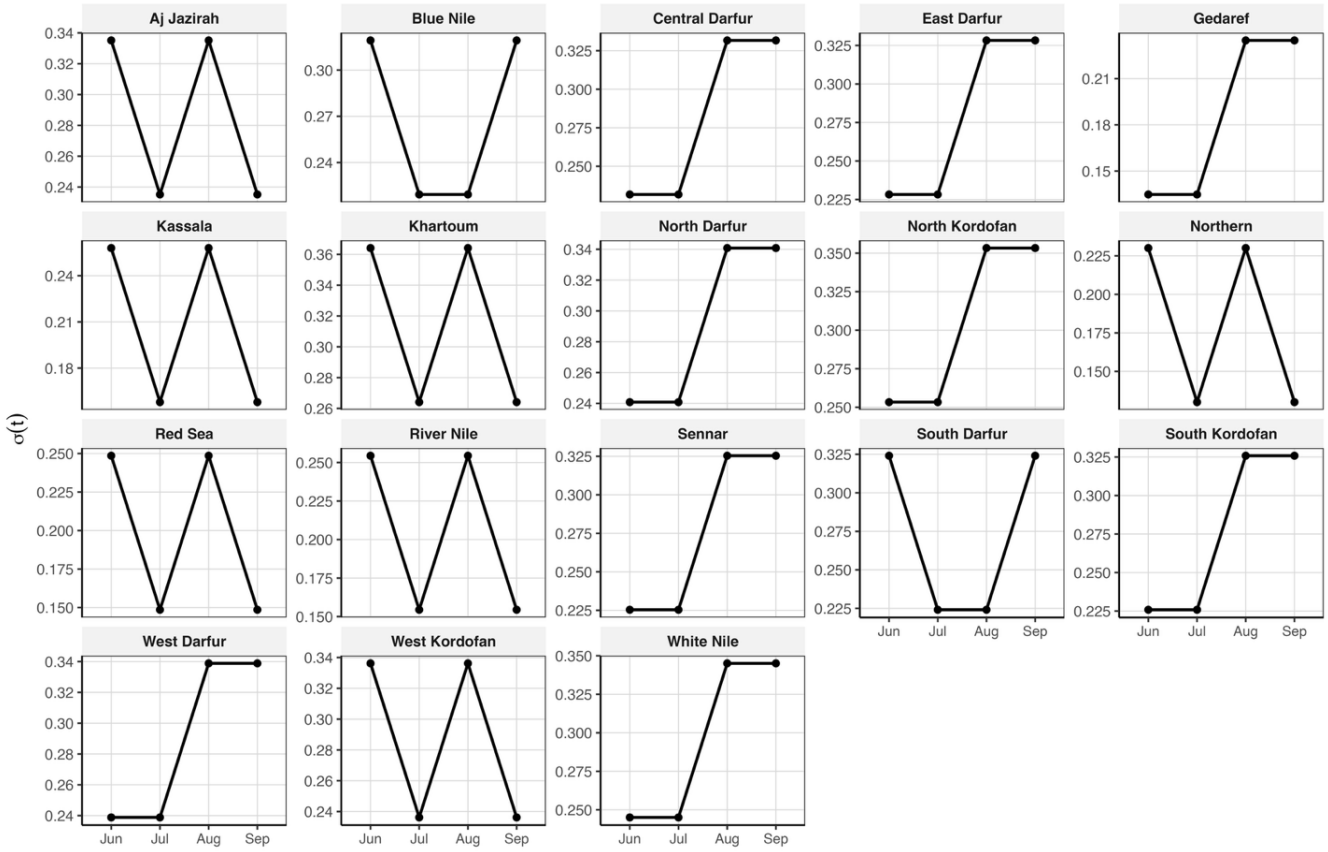

Figure 3. State-level temporal profiles of shock volatility $\sigma(t)$ from June to September. Volatility integrates the effects of conflict presence, rainfall extremes, and climatic suitability and represents the intensity of stochastic perturbations acting on the system. Higher values indicate increased uncertainty and short-term shock amplification, rather than realized impacts or losses.

Figure 4 shows the $r(t)$ across states from June to September. The urgency parameter summarizes the intensity of intervention required to maintain the policy stock constraint in the presence of biological limitations and stochastic shocks if M^{tar} is fixed as a 20% of M_t. Values of $r(t)$ close to zero indicate that the system can satisfy the policy target with minimal intervention, whereas large positive values indicate periods in which rapid action is required to counteract short-term depletion pressure. Across a majority of states (Northern, Kassala, River Nile, Red Sea, and Khartoum), inferred urgency remains near zero throughout the season, reflecting stable conditions in which biological saturation and shock volatility are insufficient to threaten the policy stock. In these regions, depletion is slow relative to uncertainty, allowing managers to rely on monitoring and routine preparedness. In contrast, several states (Blue Nile, East Darfur, South Darfur, South Kordofan, and Sennar) exhibit sharp, transient peaks in urgency, typically early in the season. These peaks coincide with periods of reduced biological saturation and elevated shock volatility, indicating that short-term losses dominate unless rapid corrective action is taken. The subsequent decline in $r(t)$ reflects improving ecological conditions or reduced stochastic pressure, rather than realized recovery. Importantly, high values of $r(t)$ do not imply observed damage, outbreak occurrence, or realized biomass loss. Instead, they represent model-implied urgency, the rate of response that would be required to prevent policy failure under prevailing conditions. As such, $r(t)$ provides a forward-looking, decision-relevant signal rather than a retrospective impact metric.

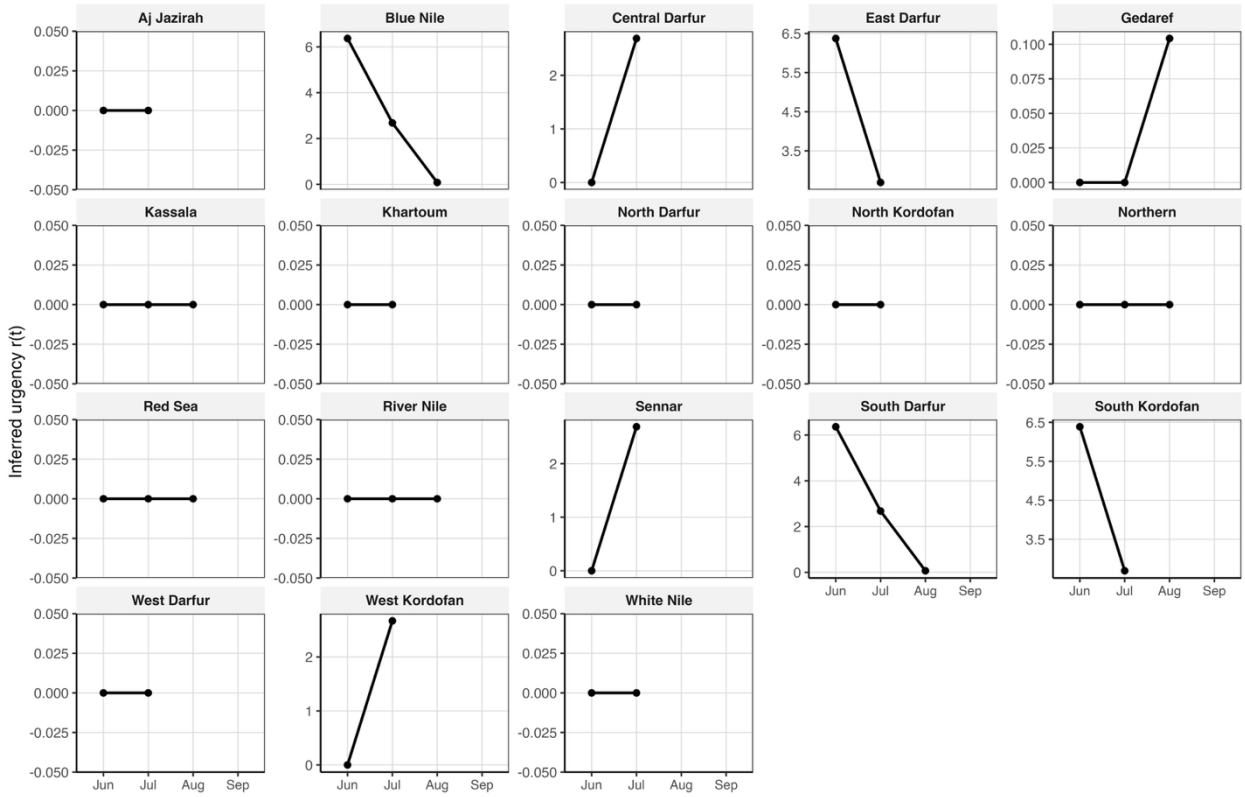

Figure 4. Temporal dynamics of inferred decision urgency $r(t)$ by state. Peaks in urgency indicate periods where rapid intervention is required to maintain the policy stock under stochastic shocks and biological constraints. Near-zero values reflect stable conditions permitting routine monitoring.

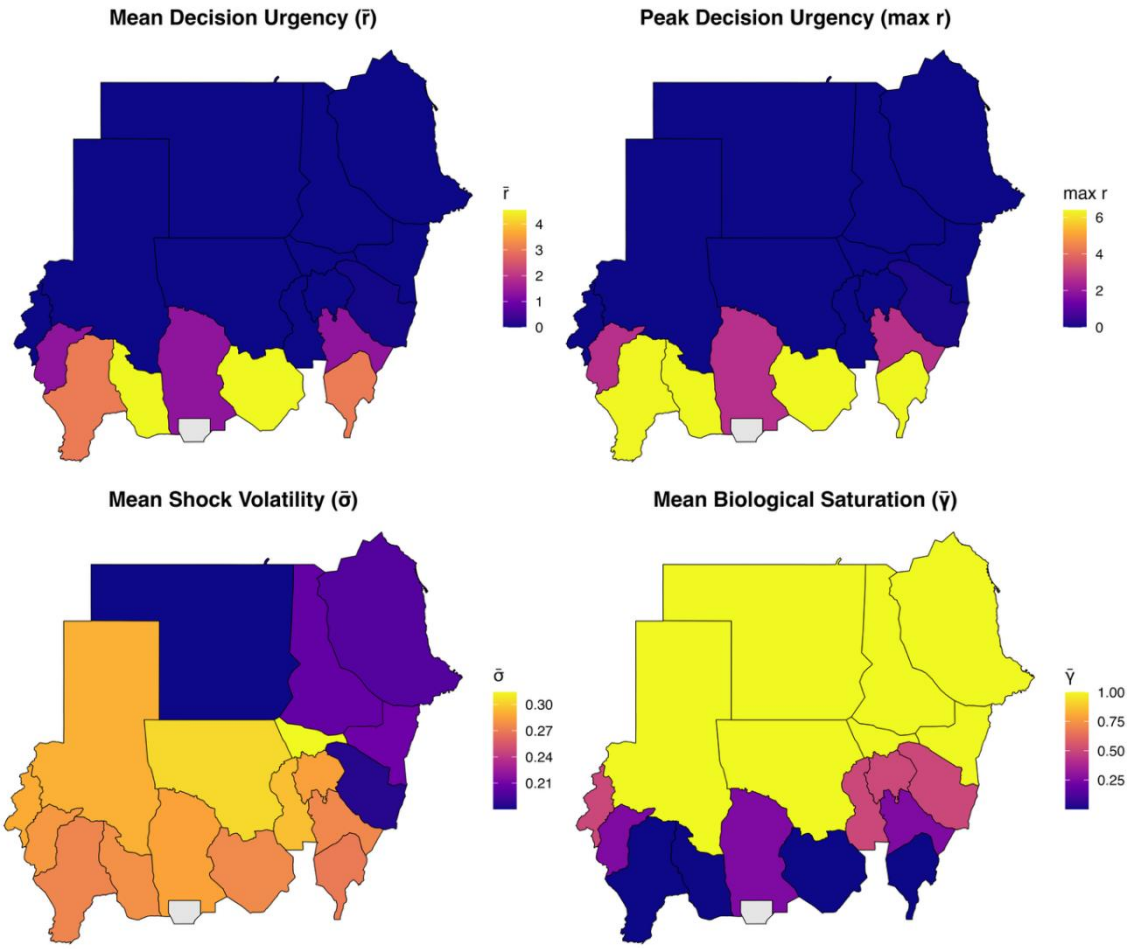

Figure 5. Spatial distribution of decision urgency and its drivers. Top panels show mean decision urgency ($\bar{r}$) and peak urgency (max r) across the season. Bottom panels display mean shock volatility ($\bar{\sigma}$) and mean biological saturation ($\bar{\gamma}$). High urgency indicates locations where rapid intervention would be required to maintain policy stock targets under stochastic shocks, rather than areas of observed impact.

Figure 5 presents the spatial distribution of decision urgency and its underlying components, aggregated at the administrative level. The upper panels show the mean inferred urgency ($\bar{r}$) and peak urgency (max r), summarizing typical and worst-case intervention pressure over the season, respectively. The lower panels display the corresponding mean shock volatility ($\bar{\sigma}$) and mean biological saturation ($\bar{\gamma}$), which jointly determine the urgency dynamics. The $\bar{r}$ is low across most northern and central regions, indicating that, on average, policy stock targets can be maintained without sustained intervention. In contrast, several southern and transitional states exhibit elevated mean urgency, reflecting persistent exposure to ecological conditions in which biological capacity is limited, and stochastic shocks exert stronger influence. The max r further reveals that even where average conditions appear stable, short but intense periods of high intervention pressure can occur, emphasizing the importance of preparedness for episodic risk rather than reliance on seasonal averages alone. Moreover, spatial patterns in urgency are closely aligned with its drivers. Regions with higher $\bar{\sigma}$ arising from conflict exposure, rainfall extremes, or environmental suitability tend to coincide with

areas of elevated peak urgency. Conversely, regions characterized by high $\bar{\gamma}$, indicating greater NDVI-derived biomass availability relative to consumption pressure, generally exhibit lower urgency despite exposure to shocks.

Figure 6 summarizes spatial variation in decision urgency using four policy-relevant classes derived from the empirical distribution of inferred urgency. Most northern and central states are classified as low urgency, indicating that ecological conditions enable the policy stock target to be maintained without immediate intervention. These regions are characterized by relatively high biological saturation and/or low shock volatility, such that depletion proceeds slowly relative to uncertainty. In contrast, several southern states fall into moderate to high urgency classes, reflecting environments where the policy stock constraint is approaching binding under plausible shock realizations. These regions warrant increased surveillance and preparedness, as modest deterioration in environmental conditions or conflict intensity could rapidly elevate intervention needs. A subset of states is classified as critical urgency, indicating that short-term depletion pressure dominates and that maintaining the policy stock target would require immediate, coordinated action. Areas labeled NA reflect insufficient or incomplete data and are excluded from interpretation. Importantly, these urgency classes do not represent observed damage, outbreak occurrence, or realized biomass loss. Rather, they identify locations where decision pressure is highest to prevent unacceptable depletion, conditional on NDVI-derived biomass dynamics and stochastic environmental shocks. Consequently, regions classified as critical urgency are not necessarily areas of highest hazard presence, but those where proactive intervention is most strongly required to meet management objectives.

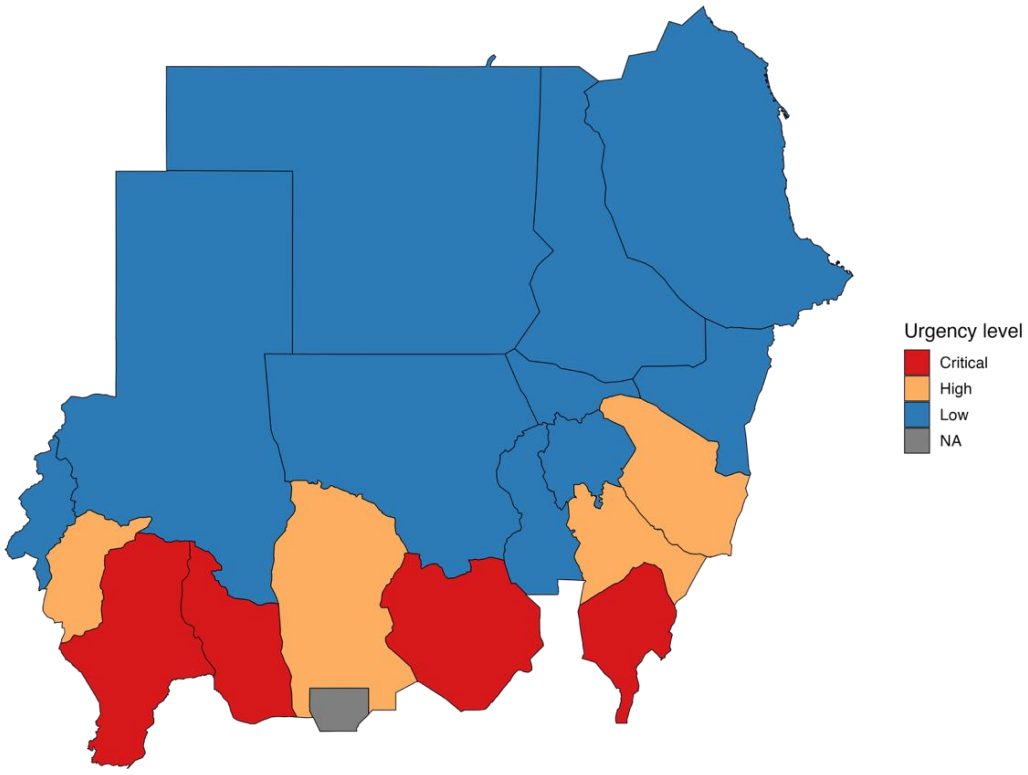

Figure 6. Spatial classification of decision urgency. Administrative units are grouped into low, moderate, high, and critical urgency classes based on quantiles of inferred urgency. Classes indicate the relative need for intervention to maintain policy stock targets under stochastic ecological shocks, rather than observed impact or realized biomass loss.

4. Discussion

In this study, we advance the translation of stochastic ecological theory into an operational decision-support framework by reformulating a Hamiltonian-based control problem into an interpretable measure of decision urgency. Classical formulations based on Hamilton–Jacobi–Bellman equations and stochastic differential dynamics provide a rigorous description of optimal control under uncertainty [43–45], but they remain difficult to operationalize for real-world management due to their abstract mathematical form and limited interpretability for practitioners. By inverting a closed-form stock kernel and expressing the solution as a time- and space-resolved urgency metric, this work bridges that gap, transforming a theoretically grounded stochastic control problem into outputs that can directly inform policy prioritization.

A key innovation of the proposed framework lies in its conceptual separation between hazard presence and decision urgency. The inferred urgency does not represent pest abundance, outbreak probability, or realized damage. Instead, it quantifies the risk of failing to maintain a policy-defined biomass stock threshold, derived from NDVI-based proxies, under prevailing ecological conditions and stochastic shocks. This distinction is critical: regions classified as high or critical urgency are not necessarily areas of highest pest pressure, but rather locations where the system is most vulnerable to rapid biomass depletion relative to the chosen management target. In this sense, the model provides a forward-looking, preventive perspective, emphasizing where timely action is most needed to avoid unacceptable losses. Under this reinterpretation, r, traditionally used to weigh future outcomes [14], represents an exogenous economic preference or subjective valuation of time, but instead quantifies the minimum urgency of intervention implied by stochastic ecological conditions.

In classical formulations, r represents an exogenous economic preference governing intertemporal trade-offs. However, because discounting directly controls how future system states influence present decisions, it also implicitly determines the temporal responsiveness of optimal control trajectories [17]. By inverting the control problem under a binding stock constraint, we leverage this structural role to reinterpret r as an endogenous indicator of decision urgency, reflecting the intensity of response required to maintain system viability under stochastic forcing. Importantly, the proposed reinterpretation does not modify the mathematical structure of stochastic control but rather exploits the intrinsic role of r in governing temporal trade-offs and trajectory sensitivity.

Another innovation of this framework is the explicit propagation of uncertainty into two biologically and operationally meaningful components. Uncertainty in the functional response parameter is treated as biological uncertainty arising from imperfect knowledge of feeding saturation and trait scaling and is propagated through uncertain allometric relationships drawn from published meta-analyses, with outcomes summarized using expectations and quantiles [39]. In contrast, the time-varying volatility parameter represents process-level instability driven by environmental and operational shocks, including rainfall extremes, desert locust suitability, and conflict-related surveillance disruptions. Redefining the volatility parameter as a bounded, interpretable instability index rather than a purely statistical noise term is particularly relevant for desert locust systems, where abrupt changes are often externally driven.

The results showed seasonal and spatial contrasts in how biological capacity and external shocks shape management pressure across Sudan (Figure 2–6). Early in the season, several agriculturally productive states exhibit strong biological buffering associated with high vegetation availability, while arid regions remain persistently resource-limited with little seasonal change. As the season progresses,

declining vegetation combined with rainfall extremes and operational disruptions increases system instability in parts of central and southern Sudan. Decision urgency rises only where these pressures coincide, producing short but pronounced periods in which rapid intervention would be required to prevent unacceptable depletion. In contrast, most northern and central states remain stable throughout the season, enabling reliance on routine monitoring rather than emergency action. These developments align with work in operations research and decision science, emphasizing the need for interpretable and robust decision-support tools under uncertainty [46–50]. Importantly, the results presented are conditional on a user-defined policy target, expressed as a fraction of baseline biomass. In this study, the target is fixed for illustrative purposes, but the framework is explicitly designed to be flexible: Decision-makers can readily adjust the target threshold to reflect different risk tolerances, management objectives, or socio-economic constraints. As such, the urgency maps should not be viewed as fixed risk products, but as adaptive decision layers that evolve with policy priorities. This flexibility is particularly relevant in operational contexts, where acceptable levels of loss may vary across regions, seasons, or governance settings.

Although this application focuses on biomass loss derived from NDVI, the framework is readily generalizable. In principle, any system in which losses can be summarized as a stock (e.g., crop yield, forage availability, ecosystem services, or economic assets), can be embedded within the same Hamiltonian structure [13]. The stock variable in this study represents the quantity that policy seeks to preserve, while stochastic drivers capture environmental, climatic, or socio-political uncertainty. This generality positions the framework as a unifying approach for decision-support across domains of environmental and agricultural management. Moreover, the construction of the stochastic volatility term assumes equal weighting of conflict, rainfall extremes, and suitability, reflecting a neutral baseline in the absence of strong prior information. However, this choice is not prescriptive. The weighting scheme can be readily adapted using expert elicitation, empirical calibration, or context-specific knowledge to emphasize particular drivers of uncertainty [51]. This adaptability enables the framework to evolve from a generic decision-support tool into a locally tailored system, aligned with stakeholder expertise and operational realities.

Moreover, the construction of the stochastic volatility term assumes equal weighting of conflict, rainfall extremes, and climatic suitability, reflecting a neutral baseline in the absence of strong prior information. In composite indicator frameworks, equal weighting is commonly adopted when empirical or theoretical evidence is insufficient to justify differential importance among components [52,53]. While this approach ensures transparency and avoids introducing subjective bias, it implicitly assumes that all contributing factors have comparable influence, which may not hold in all contexts [40]. Importantly, the choice of weights is known to influence the magnitude and interpretation of composite indicators, and different weighting schemes can lead to variation in model outputs and rankings [41]. For this reason, sensitivity analysis is widely recommended as a critical step in the construction and evaluation of composite indices to assess robustness under alternative weighting assumptions. In this framework, the equal-weighting specification should therefore be interpreted as a baseline, non-informative assumption rather than a definitive representation of system dynamics. The model is inherently flexible, and weights can be readily adjusted to reflect expert knowledge, empirical calibration, or context-specific priorities. Future extensions could systematically explore alternative weighting schemes and their influence on inferred urgency patterns, providing a more comprehensive assessment of uncertainty associated with model structure.

Nevertheless, a key limitation of this analysis arises from the use of aggregated spatial units.

Aggregating environmental and ecological processes at the administrative level may obscure important local heterogeneity, particularly in systems such as desert locust dynamics, where vegetation conditions and outbreak intensity can vary at much finer spatial scales. This issue is closely related to the MAUP, a well-established source of bias in spatial analysis, whereby statistical relationships and spatial patterns depend on the scale and zoning of aggregation [42]. In this study, the use of administrative units is motivated by the availability and harmonization of input datasets, as well as the need to align outputs with policy-relevant decision scales. However, the proposed framework is not inherently tied to this level of aggregation. It is fully scalable and can be implemented at finer spatial resolutions (e.g., gridded remote sensing data) where data availability permits. In future work, researchers should therefore explore multi-scale implementations and explicitly assess sensitivity to spatial resolution to quantify the robustness of inferred urgency patterns under alternative spatial representations. Another limitation of the present framework is that uncertainty in the biological saturation parameter $\gamma(t)$, arising from the Holling-type functional response and allometric scaling relationships, is not propagated through the inversion procedure. While $\gamma(t)$ is estimated with uncertainty and visualized using confidence bands, the inversion is performed using its mean trajectory. Consequently, the reported urgency estimates capture stochastic variability associated with environmental and operational shocks, but do not reflect uncertainty in biological response parameters. Researchers could extend the framework by propagating γ uncertainty through the inversion step, yielding distributions of $r(t)$ and enabling a more comprehensive quantification of uncertainty in decision urgency.

More broadly, this work contributes to ecological complexity research by demonstrating how stochastic process models can be operationalized without overclaiming predictive precision [54]. Rather than emphasizing individual sample paths or exact forecasts, we focus on conditional expectations, uncertainty bands, and scenario contrasts that preserve the influence of randomness while remaining interpretable [55]. The proposed reinterpretation is intentionally generic and transferable, enabling similar frameworks to be applied to other ecological disturbances, including pest outbreaks, disease emergence, or climate-driven resource shocks. In doing so, we position stochastic control not as an optimization doctrine, but as a translation mechanism between ecological uncertainty and decision-relevant insight. This shift in perspective enables stochastic models to better serve their intended role in complex ecological systems; supporting timely, transparent, and adaptive decision-making efforts under extreme uncertainty.

5. Conclusions

This study demonstrates how stochastic optimal control models, traditionally interpreted as normative optimization tools, can be re-purposed as diagnostic instruments for decision-making under extreme ecological uncertainty. By reinterpreting key control parameters as emergent indicators of decision urgency rather than fixed economic or biological constants, we bridge a critical gap between mathematical elegance and operational relevance. Applied to desert locust–driven vegetation biomass depletion in Sudan, the framework integrates biologically grounded nonlinear consumption, remotely sensed environmental variability, and operational disruption within a unified stochastic process representation. Inverting the closed-form solution of the stochastic control problem enables urgency to be inferred directly from target constraints, producing interpretable temporal and spatial patterns without relying on realized loss trajectories or equilibrium assumptions. More broadly, the proposed

reinterpretation expands the role of stochastic control theory beyond optimal exploitation problems. It provides a scalable and transferable approach for translating ecological variability and uncertainty into decision-relevant indicators of response timing and prioritization. This perspective opens new avenues for applying stochastic process models to ecological crises, disease outbreaks, and other systems in which urgency, rather than long-term optimality, is the main concern.

Acknowledgments

The authors sincerely appreciate the financial support provided by the Swedish International Development Cooperation Agency (Sida); the Swiss Agency for Development and Cooperation (SDC); the Australian Centre for International Agricultural Research (ACIAR); the Government of Norway; the German Federal Ministry for Economic Cooperation and Development (BMZ); and the Government of the Republic of Kenya.

Use of AI tools declaration

The authors declare they have not used Artificial Intelligence (AI) tools in the creation of this article.

Conflict of interest

The authors have no relevant financial or non-financial interests to disclose.

Data availability

The data used in this study are secondary and derived from publicly available sources, all of which are fully cited within the article. No new primary datasets were generated. All data processing workflows, analytical scripts, and figure-generation code used to produce the results reported in this study are openly available via GitHub and have been permanently archived on Zenodo: KOMI MENSAH AGBOKA. (2026). komimensah/Inferring-decision-urgency-from-vegetation-biomass-dynamics: A Stochastic Process Framework for Decision Urgency in Ecologically Loose Systems (0.01). Zenodo. https://doi.org/10.5281/zenodo.18445259.

References

1. M. Schlüter, R. R. J. McAllister, R. Arlinghaus, N. Bunnefeld, K. Eisenack, F. Hölker, et al., New horizons for managing the environment: A review of coupled social-ecological systems modeling, *Nat. Resour. Model.*, **25** (2012), 219–272. https://doi.org/10.1111/j.1939-7445.2011.00108.x
2. A. S. Mori, Ecosystem management based on natural disturbances: Hierarchical context and non-equilibrium paradigm, *J. Appl. Ecol.*, **48** (2011), 280–292. https://doi.org/10.1111/j.1365-2664.2010.01956.x
3. S. A. Vollert, C. Drovandi, M. P. Adams, Ecosystem knowledge should replace coexistence and stability assumptions in ecological network modelling, *Bull. Math. Biol.*, **87** (2025), 17. https://doi.org/10.1007/s11538-024-01407-9
4. J. Aber, R. P. Neilson, S. McNulty, J. M. Lenihan, D. Bachelet, R. J. Drapek, Forest processes

and global environmental change: Predicting the effects of individual and multiple stressors: We review the effects of several rapidly changing environmental drivers on ecosystem function, discuss interactions among them, and summarize predicted changes in productivity, carbon storage, and water balance, *Bioscience*, **51** (2001), 735–751. https://doi.org/10.1641/0006-3568(2001)051[0735:FPAGEC]2.0.CO;2

5. M. Taherkhani, Evaluating factors influencing insect outbreak case study (invasion of locusts), Sustain, *Earth Trends*, **2** (2022), 30–41. https://doi.org/10.48308/sustainearth.2022.101842
6. D. J. Wilkinson, Stochastic modelling for systems biology, 2nd edition, Chapman & Hall/CRC, (2011). https://doi.org/10.1080/09332480.2012.752295
7. O. C. Ibe, Markov processes for stochastic modeling, 2nd edition, Elsevier Inc., (2013). https://doi.org/10.1016/C2012-0-06106-6
8. N. Chen, Stochastic methods for modeling and predicting complex dynamical systems: Uncertainty quantification, state estimation, and reduced-order models, 2nd Edition, Springer Cham, (2025). https://doi.org/10.1007/978-3-031-81924-7
9. N. Touzi, Optimal stochastic control, stochastic target problems, and backward SDE, 2010. Available from: https://link.springer.com/book/10.1007/978-1-4614-4286-8
10. T. Björk, Arbitrage theory in continuous time, 2nd edition, Oxford University Press Inc., (2005). https://doi.org/10.1093/0199271267.001.0001
11. G. Fabbri, F. Gozzi, A. Swiech, Stochastic optimal control in infinite dimension: Dynamic programming and HJB equations, in: *Probability and stochastic modelling* (eds. S. Asmussen, P. W. Glynn and Y. L. Jan), Springer, 2017. https://doi.org/10.1007/978-3-319-53067-3
12. Thakur T, Stochastic Calculus and Brownian Motion, Educohack Press, 2025.
13. J. Yong, X. Y. Zhou, Stochastic controls: Hamiltonian systems and HJB equations, in: *Applications of Mathematics* (eds. I. Karatzas and M. Yor), Springer, (1999). https://doi.org/10.1007/978-1-4612-1466-3
14. A. S. Diallo, S. B. Affognon, B. M. Ndiaye, P. Ngare, Stochastic optimal control and simulations with application to the cashew nut sector in Senegal, *Results Appl. Math.*, **14** (2022), 100272. https://doi.org/10.1016/j.rinam.2022.100272
15. S. Bajpai, A. Sameer, The dynamics of uncertainty: A systematic review of non-linear dynamical systems in decision-making, *Nonlinear Dyn.*, **113** (2025), 18951–18967. https://doi.org/10.1007/s11071-025-11180-6
16. D. Tuckett, A. Mandel, D. Mangalagiu, A. Abramson, J. Hinkel, K. Katsikopoulos, et al., Uncertainty, decision science, and policy making: A manifesto for a research agenda, *Crit. Rev.,* **27** (2015). https://doi.org/10.1080/08913811.2015.1037078
17. J. K-H. Quah, B. Strulovici, Discounting, values, and decisions, *J. Pol. Econ.*, **121** (2013), 896–939. https://doi.org/10.1086/673867
18. G. dos Reis, D. Šiška, Stochastic control and dynamic asset allocation, 2025. Available from: https://webhomes.maths.ed.ac.uk/~dsiska/LecNotesSCDAA.pdf
19. S. J. Simpson, A journey towards an integrated understanding of behavioural phase change in locusts, *J. Insect. Physiol.*, **138** (2022), 104370. https://doi.org/10.1016/j.jinsphys.2022.104370
20. E. Despland, S. J. Simpson, The role of food distribution and nutritional quality in behavioural phase change in the desert locust, *Anim. Behav.*, **59** (2000), 643–652. https://doi.org/10.1006/anbe.1999.1335
21. S. J. Simpson, A. R. McCaffery, B. F. HÄgele, A behavioural analysis of phase change in the desert locust, *Biol. Rev.*, **74** (1999), 461–480. https://doi.org/10.1111/j.1469-185X.1999.tb00038.x

22. G. E. Baraka, G. D'Urso, O. R. Belfiore, The application of earth observation data to desert locust risk management: A literature review, *Geomatics*, **5** (2025), 14. https://doi.org/10.3390/geomatics5010014
23. T. K. Babar, Risks of deserts locust and its mitigation, in: *Disaster Risk Reduction in Agriculture. Disaster Resilience and Green Growth* (eds. M. Ahmed and S. Ahmad), Springer, (2023), 361–392. https://doi.org/10.1007/978-981-99-1763-1_17
24. X. Liu, D. Zhang, X. He, Unveiling the role of climate in spatially synchronized locust outbreak risks, *Sci. Adv.*, **10** (2024), eadj1164. https://doi.org/10.1126/sciadv.adj1164
25. I. Klein, N. Oppelt, C. Kuenzer, Application of remote sensing data for locust research and management—a review, *Insects*, **12** (2021), 233. https://doi.org/10.3390/insects12030233
26. C. S. Holling, Some characteristics of simple types of predation and parasitism, *Can. Entomol.*, **91** (1959): 385–398. https://doi.org/10.4039/Ent91385-7
27. E. Kimathi, H. E. Z. Tonnang, S. Subramanian, K. Cressman, E. M. Abdel-Rahman, M. Tesfayohannes, et al., Prediction of breeding regions for the desert locust Schistocerca gregaria in East Africa, *Sci. Rep.*, **10** (2020), 11937. https://doi.org/10.1038/s41598-020-68895-2
28. B. M. Sokame, K. M. Agboka, E. Kimathi, B. T. Mudereri, E. M. Abdel-Rahman, T. Landmann, et al., An integrated assessment approach for socio-economic implications of the desert locust in Eastern Africa, *Earths Futur.*, **12** (2024), e2023EF003841. https://doi.org/10.1029/2023EF003841
29. K. M. Agboka, E. M. Abdel-Rahman, E. Kimathi, B. M. Sokame, T. Landman, S. Niassy, et al., Prediction of recurrent desert locust invasions under climate variability in the extended Sahara desert: An evolutionary adaptive Neuro-Fuzzy approach, *Int. J. Trop. Insect. Sci.*, **46** (2025), 571–580. https://doi.org/10.1007/s42690-025-01705-2
30. T. Landmann, K. M. Agboka, I. Klein, E. M. Abdel-Rahman, E. Kimathi, B. T. Mudereri, et al., Towards early response to desert locust swarming in eastern Africa by estimating timing of hatching, *Ecol. Modell.*, **484** (2023), 110476. https://doi.org/10.1016/j.ecolmodel.2023.110476
31. N. Mohamed, B. Abderrazak, The relationship between vegetation and rainfall in central Sudan, *Int. J. Remote Sens.*, **6** (2016), 30–40. https://doi.org/10.14355/ijrsa.2016.06.004
32. A. T. Showler, M. Lecoq, Incidence and ramifications of armed conflict in countries with major desert locust breeding areas, *Agronomy*, **11** (2021), 114. https://doi.org/10.3390/agronomy11010114
33. D. M. Becker, Behavior of discount rates in present value calculation, *Int. J. Financ. Eng.*, **12** (2025), 2550025. https://doi.org/10.1142/S2424786325500252
34. A. Pierru, E. Feuillet-Midrier, Discount rate value and cash flow definition: A new relationship and its implications, *Eng. Econ.*, **47** (2002), 60–74. https://doi.org/10.1080/00137910208965023
35. C. Gollier, P. Koundouri, T. Pantelidis, Declining discount rates: Economic justifications and implications for long-run policy, *Econ. Policy*, **23** (2008), 758–795. https://doi.org/10.1111/j.1468-0327.2008.00211.x
36. R.G. Newell, W. A. Pizer, Uncertain discount rates in climate policy analysis, *Energy Policy*, **32** (2004), 519–529. https://doi.org/10.1016/S0301-4215(03)00153-8
37. Centre de Suivi Écologique (CSE). Rapport technique – année 2011. Dakar: 2011.
38. M. Diankha, K. O. Hackman, S. M. Sarr, The use of Normalized Difference Vegetation Index (NDVI) to assess urban forests dynamics in West Africa: A case study of Mbao Classified Forest, Dakar (Senegal) 2022. Available from: https://openknowledge.fao.org/handle/20.500.14283/cc1263en

39. G. Englund, G. Öhlund, C. L. Hein, S. Diehl, Temperature dependence of the functional response, *Ecol. Lett.*, **14** (2011), 914–921. https://doi.org/10.1111/j.1461-0248.2011.01661.x
40. C. Wehbe, H. Baroud, Limitations and considerations of using composite indicators to measure vulnerability to natural hazards, *Sci. Rep.*, **14** (2024), 19333. https://doi.org/10.1038/s41598-024-68060-z
41. N. Valizadeh, D. Hayati, Formulating indicator selection and composite index validation and application system for agricultural sustainability assessment, *Results Eng.*, **28** (2025), 106978. https://doi.org/10.1016/j.rineng.2025.106978
42. M. Buzzelli, Modifiable areal unit problem, *Int. Encycl. Hum. Geogr.*, (2019), 169–173. https://doi.org/10.1016/B978-0-08-102295-5.10406-8
43. C. S. Della, R. C. Kraaij, Large deviations for Markov processes with switching and homogenisation via Hamilton–Jacobi–Bellman equations, *Stoch. Process. Appl.,* **170** (2024): 104301. https://doi.org/10.1016/j.spa.2024.104301
44. E. Bandini, C. Keller, Non-local Hamilton–Jacobi–Bellman equations for the stochastic optimal control of path-dependent piecewise deterministic processes, *Stoch. Process. Appl.*, **192** (2026), 104813. https://doi.org/10.1016/j.spa.2025.104813
45. J. Qiu, Weak solution for a class of fully nonlinear stochastic Hamilton–Jacobi–Bellman equations, *Stoch. Process. Appl.*, **127** (2017), 1926–1959. https://doi.org/10.1016/j.spa.2016.09.010
46. M. D. A. Rounsevell, A. Arneth, C. Brown, W. W. L. Cheung, O. Gimenez, I. Holman, et al., Identifying uncertainties in scenarios and models of socio-ecological systems in support of decision-making, *One Earth*, **4** (2021), 967–985. https://doi.org/10.1016/j.oneear.2021.06.003
47. A. B. Barrett, S. Duivenvoorden, E. E. Salakpi, J. M. Muthoka, J. Mwangi, S. Oliver, et al., Forecasting vegetation condition for drought early warning systems in pastoral communities in Kenya, *Remote Sens. Environ.*, **248** (2020), 111886. https://doi.org/10.1016/j.rse.2020.111886
48. X. Wang, Y. Li, S. Zhang, The interplay between green product production and advertising investment under green reputation, *IEEE Trans. Eng. Manag.*, **77** (2025), 2680–2699. https://doi.org/10.1109/TEM.2025.3582257
49. A. K. Kwarteng, A. A. Bulti, A. Teka, Quantifying vegetation responses to rainfall extremes in Sub-Saharan Africa using CHIRPS precipitation and MODIS NDVI, *Remote Sens.*, **18** (2026), 768. https://doi.org/10.3390/rs18050768
50. X. Wang, Y. Zhang, S. Zhang, Dynamic order allocation in a duopoly hybrid workforce of competition: A machine learning approach, *Eur. J. Oper. Res.*, **315** (2024), 668–690. https://doi.org/10.1016/j.ejor.2023.12.026
51. K. M. Agboka, J. T. C. Ouaba, F. Meutchieye, T. Tchuinkam, T. Landmann, E. M. Abdel-Rahman, et al., Using a knowledge representation logic to estimate the availability of Imbrasia epimethea (Lepidoptera: Saturniidae), an important edible insect in Sub-Saharan Africa, *Ecol. Inform.*, **84** (2024), 102890. https://doi.org/10.1016/j.ecoinf.2024.102890
52. M. Mazziotta, A. Pareto, Complexity in society: From indicators construction to their synthesis, in: *Social Indicators Research Series* (ed. F. Maggino), Springer, **70** (2017). https://doi.org/10.1007/978-3-319-60595-1
53. S. Greco, A. Ishizaka, M. Tasiou, G. Torrisi, On the methodological framework of composite indices: A review of the issues of weighting, aggregation, and robustness, *Soc. Indic. Res.*, **141** (2019), 61–94. https://doi.org/10.1007/s11205-017-1832-9
54. C. A. Malmborg, A. M. Willson, L. Bradley, M. A. Beatty, D. H. Klinges, G. Koren, et al., Defining model complexity: An ecological perspective, *Meteorol. Appl.*, **31** (2024), e2202.

https://doi.org/10.1002/met.2202
55. R. L. Winkler, Y. Grushka-Cockayne, K. C. Lichtendahl, V. R. R. Jose, Probability forecasts and their combination: A research perspective, *Decis. Anal.*, **16** (2019), 239–333. https://doi.org/10.1287/deca.2019.0391

AIMS Press